Electrocatalysis in confinement: metal-organic frameworks for oxygen reduction

Hoefnagel, M.E.

Chapter 1

Introduction

The Role of Metal-Organic Framework Induced Confinement Effects on Molecular Electrocatalysts Relevant to the Energy Transition

Metal-Organic Frameworks (MOFs) are promising materials for (electro)catalysis as they can improve stability, reusability and catalytic current densities of molecular catalysts, thereby combining the advantages of homogeneous- and heterogeneous catalysts. However, much is unknown about the effects of confinement of a catalyst within a MOF on the overall catalytic behavior. We compare the performance of a series of electrocatalysts confined in MOFs to that of the corresponding homogeneous catalysts to evaluate to what extent the catalytic site is affected by confinement in terms of stability, activity and selectivity. Together the examples discussed depict what happens to a catalyst when it is incorporated into a MOF, and recommendations are made on how to evaluate the electrochemical activity of a MOF in a way that allows for description of such confinement effects on the catalyst performance. We note that the limiting factor for the catalytic reaction in MOFs is found in 1) slow electron transport, 2) slow mass transport of reactants and products, or 3) a low activity of the catalytic site itself. Understanding the changes in mass transport and electron transport and the resulting effects on catalytic mechanism is essential to be able to bring MOF systems to practical applications.

This chapter was published as a review article: M. E. Hoefnagel, D. G. H. Hetterscheid, *ChemSusChem* **2025**, 18, e202402676.

1.1 Electrocatalysis and the energy transition

The climate crisis is largely caused by the combustion of fossil fuels to meet energy demands. Combustion of fossil fuels releases greenhouse gasses that result in an increase of temperature, melting of land- and sea ice, ocean acidification, loss of biodiversity, draughts, forest fires and more.[1,2] The effects of climate change hit hardest to those in underdeveloped regions, further increasing their vulnerability. Simultaneously, the number of people with access to the energy market is rapidly increasing and therefore so is the amount of energy needed.[3] With 16200 TW per year the sun provides an abundant amount of energy to meet all our demands.[4] However, the intermittent availability of sunlight gives rise to the need to store the energy obtained from solar cells. Solar energy is converted to chemical energy by the synthesis of fuels. Production of fuels can either proceed directly by photochemical approaches, or sequentially by photovoltaics and electrolysis. The electricity generated by photovoltaics may also be stored in batteries, albeit the energy density of most battery systems is low.[5] Suitable fuels consist of small molecules such as molecular hydrogen that is produced by electrochemical water splitting, and carbon-based fuels that are obtained by CO_2 reduction.[6] Electrocatalysis is expected to play a significant role in the shift from a fossil fuel-based economy to a more renewable energy economy.[7,8] The most common electrocatalytic reactions that are relevant for renewable energies are hydrogen evolution (eq. 1), water oxidation (eq. 2), carbon dioxide reduction (eq. 3 and 4) and oxygen reduction (eq. 5 and 6).

Hydrogen evolution

The 4-electron reduction of protons to yield molecular hydrogen is one of the electrochemical half reactions in water splitting and has a standard equilibrium potential (E°) of 0 V versus the Standard Hydrogen Electrode (SHE). Platinum-based heterogeneous catalysts are currently the most common catalysts for the hydrogen evolution reaction (HER) due to their high hydrogen yields and low overpotential.[9–11] However, the use of platinum is costly and the field is moving towards low cost, efficient catalysts based on earth abundant metals.[12,13]

$$4H^+ + 4e^- \longrightarrow H_2 \qquad E° = 0\ V \qquad (1)$$

Water oxidation

The second, and thermodynamically most challenging half reaction in water splitting is the 4-electron oxidation of water into dioxygen and protons. With a standard equilibrium potential of 1.23 V vs. SHE, catalysts for the water oxidation reaction (WOR) need to be able to lower the energy barrier for this reaction significantly. Catalysts for the WOR are often Ir-based and Ru-based metal complexes or metal oxides, but many efforts are being made for the design of first-row transition metal complexes and oxides for water oxidation, mostly based on Co, Mn and Cu.[14–16]

$$2\ H_2O \longrightarrow O_2 + 4H^+ + 4e^- \qquad E° = 1.23\ V \qquad (2)$$

CO_2 reduction

CO_2 reduction mostly refers to the 2-electron reduction of CO_2 into CO and water, with an equilibrium potential of −0.52 V vs. SHE, or into formate, with an equilibrium potential of −0.61 V vs. SHE.[17] CO_2 reduction can also include the further reduction of CO into methane, methanol and multicarbon products such as ethylene. Catalysts that bind to the oxygen of CO_2 tend to produce formate and catalysts that bind to the carbon tend to produce CO. The most common heterogeneous catalysts for the CO_2 reduction reaction (CO_2RR) are Au and Ag for formation of CO, Sn for production of formate and Cu for multicarbon products.[18–20] The most common homogeneous catalysts for CO_2RR are Co-based porphyrins and phthalocyanines.[21–28]

$$CO_2 + 2H^+ + 2e^- \longrightarrow CO + H_2O \qquad E° = -0.52\ V \qquad (3)$$

$$CO_2 + H^+ + 2e^- \longrightarrow HCOO^- \qquad E° = -0.61\ V \qquad (4)$$

Oxygen reduction

The 4-electron reduction of dioxygen to water is the reverse reaction of the WOR and is the cathodic reaction in fuel cells. Alternatively, it can also be the 2-electron reduction of dioxygen to hydrogen peroxide, which in turn can be further reduced to water. Currently, the most common material for the oxygen reduction reaction (ORR) in fuel cells is platinum due to its relatively low overpotential and faradaic efficiency (FE) of 100% for water. More earth-abundant alternatives are Fe-based and Co-based heterogeneous catalysts and Cu-based and Co-based metal complexes.[29]

$$O_2 + 4H^+ + 4e^- \longrightarrow 2\ H_2O \qquad E° = 1.23\ V \qquad (5)$$

$$O_2 + 2H^+ + 2e^- \longrightarrow 2\ H_2O_2 \qquad E° = 0.7\ V \qquad (6)$$

To successfully transition to a renewable energy economy, the development of better catalysts for these reactions is indispensable. New and emerging technologies and strategies may be essential as well. Electrocatalysts can be either heterogeneous, such as materials and surfaces mostly based on metals, or homogeneous, such as coordination complexes of transition metals. Heterogeneous catalysts have the advantage of a large number of active sites at the electrode surface, allowing for large catalytic currents and high product yields.[30] However, catalytic mechanisms and the true identity of catalytically active species are often ambiguous, making optimization of material properties difficult. Homogeneous catalysts have the advantage of precise tunability of their structure and therefore allow for studying and utilizing structure-activity relationships. However, homogeneous catalysts often suffer from instability, poor recoverability, poor scalability and they are difficult to recycle.[31] Immobilization of homogeneous electrocatalysts onto electrode surfaces can help overcome these problems and combine some of the advantages of both heterogeneous and homogeneous electrocatalysts.[32] Particularly the incorporation of molecular catalysts in Metal-Organic Frameworks (MOFs) has received attention lately, due to the potential that these systems have shown thus far for catalytic purposes.

1.2 MOFs as electrocatalysts

MOFs are highly symmetrical 3D coordination polymers that consist of metal nodes and organic linkers. The high porosity of these systems results in high catalytic surface areas, and the possibility to vary the structure of the framework infinitely by alterations of the linkers and nodes make them interesting materials to tune the (electronic) structure of the catalyst in the first, second and even third coordination sphere. [33–36] This is essential given that precise tuning of the catalyst is favorable to the specific reaction that they catalyze.[37] Moreover, incorporation of catalysts into a MOF has been shown to increase the stability and reusability of the catalytic site in some occasions, as well as to influence selectivity and rates of the catalytic reaction by confinement effects in other examples.[38–40] Simultaneously, the number of active sites per unit of surface area can be pushed to numbers far beyond that of typical heterogeneous catalysts, while bimolecular reactions leading to undesired side phenomena can be shut down.

Molecular catalysts can be incorporated into MOFs by various strategies, as summarized schematically in Figure 1.1:[41] 1) A MOF can contain catalytically active nodes (Figure 1.1a) such as for example the MIL-100 framework wherein the Sc^{3+}/Fe^{3+} nodes are active for tandem C–C bond formation and alcohol oxidation;[42] 2) The catalytic site can be imbedded in the linker (Figure 1.1b), of which porphyrinic PCN frameworks are a good example. In these frameworks, four carboxylic acids moieties on the porphyrin bind to the Zr-cluster nodes;[43,44] 3) A catalyst can be trapped inside MOF pores during synthesis by the 'ship-in-a-bottle' approach (Figure 1.1e);[45] 4) Homogeneous catalysts can be introduced into the MOF by post-synthetic modification (PSM) methods. An example of PSM is post synthetic ligand exchange (Figure 1.1c), as reported for the [FeFe]-hydrogenase functionalized UiO-66 framework. Here some of the dicarboxybenzene ligands are replaced by dicarboxybenzene ligands functionalized with the [Fe-Fe]-hydrogenase catalysts, by simply stirring a solution containing the MOF in presence of the catalyst.[46] Another form of PSM is solvent assisted ligand exchange (SALI) (Figure 1.1d), where the MOF is soaked in a concentrated solution of catalyst at elevated temperatures. Within this strategy, hydroxyl groups on MOF nodes are replaced by carboxylic acid moieties on the catalyst. [24,47] The MOFs can be mounted onto electrodes to test their electrocatalytic activity. The most common method in the literature is to drop cast an ink containing the MOF, a conductive carbon support such as carbon black or multiwalled carbon nanotubes (MWCNTs) and a binder such as Nafion® or Sustainion®.[43,47–49] Alternatively, MOFs can be grown solvothermically onto FTO or ITO electrodes.[50–52]

When a catalyst is incorporated into a MOF, the aforementioned confinement effects are expected to affect the mechanism and rate-determining step of the catalytic reaction to some extent. Due to such confinement effects, for a given electrocatalytic process, the limiting factor for the overall reaction may be found in slow electron transport between the active sites and the electrode, a limited mass transport of reactants and products, or be limited by the intrinsic activity of the catalytic site itself. Electron transport is expected to be the limiting factor when the redox-active moieties are diffuse, and charge propagation is expected to depend on electron hopping from one catalytic center to another. In this case, the catalytic reaction will likely take place close to the electrode surface, where electrons are injected into the MOF. Alternatively, when mass transport of reactants and products is rate limiting, the catalytic reaction is expected to take place at the MOF – electrolyte interface where new reactants are first replenished. Lastly, if the catalytic reaction is limited by the activity of the catalyst itself, catalysis is expected to take place

throughout the entire MOF. Since the mass transport and charge transport mechanisms within the MOF are undoubtedly different from those in the homogeneous situation, a comparison between the confined catalyst and the catalyst in homogeneous solution may be very insightful. Performance of catalysts is often evaluated by turnover numbers (TONs), which represent the stability of a catalyst, and turnover frequencies (TOFs), which represent the activity of the catalyst.[53] It is however, important to note that TONs are difficult to determine for homogeneous electrocatalysts, as it requires determination of the exact number of catalytic species present at the electrode surface. This is far from straightforward to determine due to the diffusive nature of the catalytic species, which makes drawing conclusions in terms of improved stability through confinement often problematic. Nevertheless, understanding how confinement effects affect the catalytic activity, mass transport and electron transport throughout MOFs is essential to be able to bring such MOF systems to practical applications.

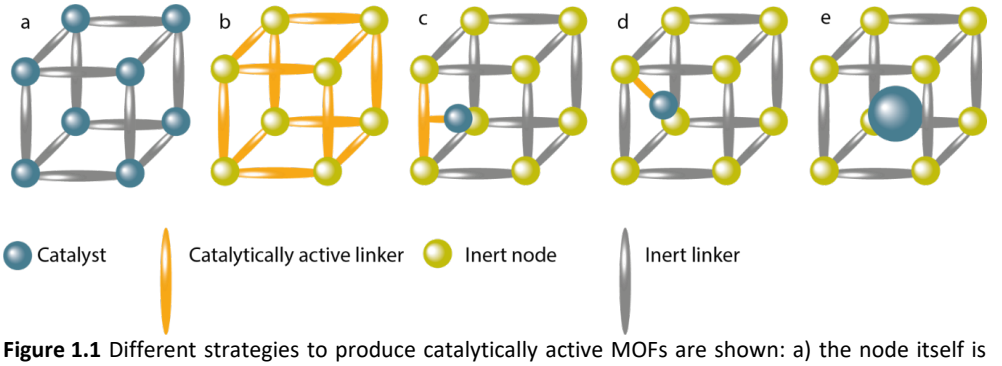

Figure 1.1 Different strategies to produce catalytically active MOFs are shown: a) the node itself is catalytically active; b) the linker is the catalyst; c) the catalyst is anchored to the linker during the synthesis or through post synthetic ligand exchange strategies; d) the catalyst is bound to the node via solvent assisted ligand incorporation; e) the catalyst is trapped in the pores via the ship-in-a-bottle approach.

Various comprehensive reviews have discussed the use of MOFs as electrocatalysts,[35] how to evaluate the electrochemical performance of these MOFs,[54] redox active MOFs for energy storage and conversion,[55] and coordination-sphere effects on MOF electrocatalysts.[34] However, a systematic evaluation of the effect of confinement on the catalyst within the MOF, and how confinement changes the overall catalytic behavior of the active site has thus far not been reported. This chapter discusses a selection of studies on molecular electrocatalysts immobilized in metal organic frameworks for catalytic reactions relevant to the energy transition.

1.3 Hydrogen evolution catalysts in MOFs

1.3.1 Cobaloxime

Cobalt complexes with diglyoxime ligands, also known as cobaloximes, are among the most intensively investigated homogeneous catalysts for the hydrogen-evolution reaction.[56] In the catalytic reaction a Co^{III} cobaloxime is reduced to a Co^{II} or Co^{I} species that is protonated to form a Co^{II}-hydride or a Co^{III}-hydride intermediate. Here the precise details depend on the electronic structure of the complex. Irrespective of whether a Co^{III}-H or Co^{II}-H cycle is operative, formation of the active hydride compound is typically the rate-determining step.

The catalytic reaction can proceed via four different pathways, either by homolytic or heterolytic H–H bond formation, and either occurring at the Co^{II}-H or Co^{III}-H species, as schematically shown in Figure 1.2. In the homolytic pathway, two Co-hydride species react in a bimolecular reaction to release dihydrogen, while in the heterolytic pathway the Co-hydride is protonated to produce H_2 and $Co^{III/II}$. The homolytic pathway proceeds via intermediates that can be generated at milder potentials and depends on the diffusion of two cobalt hydride species towards each other in solution. However, a reaction between two such species can also trigger a catalyst degradation trajectory that occurs via a bimolecular deactivation pathway.[57,58] Overreduction of the cobaloxime was found to generate carbon-based α-imino radical species that react with each other to form inactive dimers. Therefore, directing the catalytic mechanism towards the heterolytic HER pathway by immobilization of the cobaloxime is anticipated to improve the stability of the catalyst, albeit with a larger overpotential as a direct consequence. In addition to this bimolecular degradation pathway, the instability of cobaloximes may be caused by hydrogenation of the ligand triggered by a hydride migration from the Co^{I}LH species. This degradation pathway can be prevented by direct reduction of this Co^{I}LH species to the catalytically active H-Co^{II}-LH species.[57] Immobilization of the catalyst on an electrode allows for rapid reduction reactions and may prevent dimerization and can therefore slow down cobaloxime degradation, explaining the improved stability of immobilized cobaloxime catalysts compared to homogenous equivalents. Following such a strategy, cobaloximes have been immobilized on, amongst others, metal oxides, carbon nanotubes (CNT), liposomes, and MOFs.[59–62]

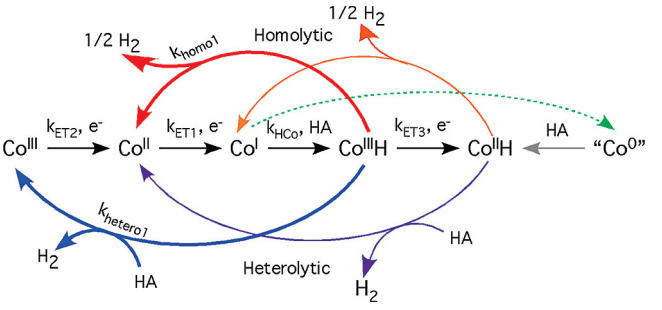

Figure 1.2 Schematic pathway of the most common pathways resulting in H_2 evolution catalyzed by cobaloximes. Figure reprinted with permission of reference 56.

In the MOF approach, cobaloxime was equipped with four benzenecarboxylic acid moieties and used as a linker in the **UU-100(Co)** MOF with hexanuclear zirconium nodes (Figure 1.3) and was studied as a catalyst for the hydrogen-evolution reaction.[52] The cobaloximes were found to promote electron transfer throughout the film, as monitored with UVvis spectroelectrochemistry and Cottrell analysis, as well as function as molecular hydrogen-evolution catalysts. High catalytic current densities were obtained during chronoamperometry at −0.45 V vs. RHE for 18 hours at pH 4, with an FE of around 80% for H_2.

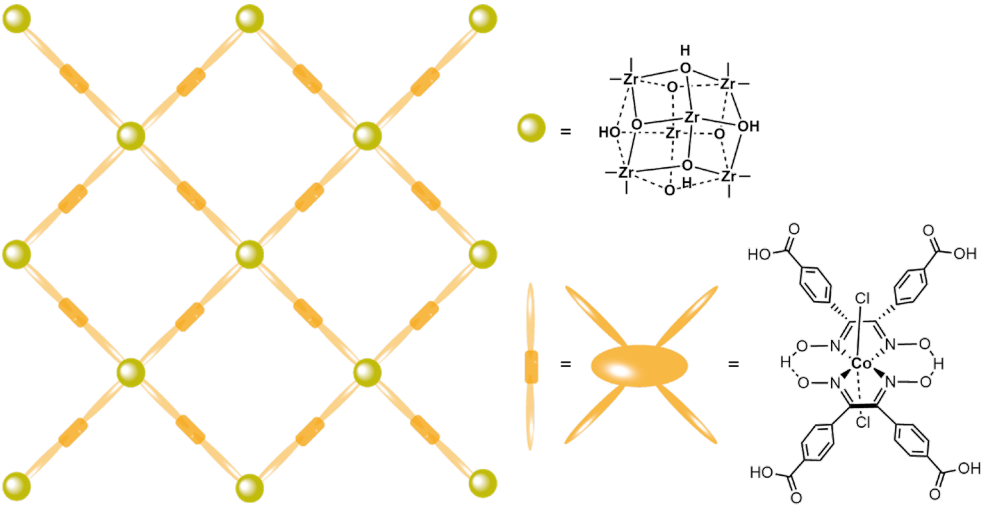

Figure 1.3 Schematic presentation of the **UU-100(Co)** MOF.

Keeping in mind the discrepancies between homogeneous and heterogeneous TONs, incorporation of the cobaloxime into the framework greatly increased its stability (Table **1.1**). The turnover number went up from 10 for the linker in homogeneous solution to more

than 20 000 when imbedded within the MOF. This was attributed to the rigid 3D structure of the MOF that rigorously prevents dimer formation. The stability of the MOF also compares favorably to that of cobaloximes immobilized on carbon nanotubes and composites of carbon nanotubes and polymers, for which TONs between 120 and 420 were obtained.[60,61] Formation of cobaloxime dimers in the rigid framework of the MOF is even more difficult than when grafted onto carbon substrates and may contribute to the large improvement in stability in the MOF embedded catalyst compared to other immobilization methods. Cobaloximes are not stable at low pH (<2.2) and complete dissociation leading to metallic depositions on the electrode have been reported.[63] Little is known regarding local pH effects within MOFs, and to which extend alkalization within the MOF pores contributes to some extent to its stability during catalysis. [64,65]

Table 1.1 TONs obtained for cobaloxime-based hydrogen evolution systems.

Species	**TON ($^{-1}$)**
Cobaloxime linker (hom)[a]	10[52]
UU-100(Co)[b]	> 20 000[52]
Cobaloxime on CNT[c]	120[60]
Cobaloxime-polymer composit on CNT[d]	420[61]

[a] −0.45 V vs. RHE, acetate buffer pH 4, WE = carbon rod, [b] −0.43 V vs. RHE, acetate buffer pH 5.3, WE = FTO, [c] −0.337 V vs. RHE, NaCl pH 7, WE = glassy carbon, [d] −0.45 V vs. RHE, phosphate buffer pH 7, WE = CNT buckypaper.

1.4 CO_2 reduction catalysts in MOFs

1.4.1 Co-phthalocyanine

Co-phthalocyanines (CoPCs) are among the most investigated and most stable homogeneous catalysts for the reduction of CO_2 to CO.[21] The mechanism of CO_2 reduction proceeds by reduction of Co^{II} to Co^{I}, binding of CO_2 and transfer of an electron from Co to CO_2. This electron transfer from Co to CO_2 is the rate-determining step and is coupled to transfer of a proton at high carbonate concentrations or followed by a separate proton transfer step at low carbonate concentrations.[66] In electrocatalytic CO_2 reduction by CoPC, the true catalytically active species is not homogeneous, but an electro-absorbed CoPC species on the electrode. Aromatic macrocycles such as phthalocyanine tend to aggregate,[66] leading to inactive oligomeric stacks. As a result, a water-soluble CoPC studied by Wu et al. in aqueous electrolyte lost more than 50% of its activity within 30 minutes due

to stacking interactions.[67] However, Warren and coworkers recently reported a water-soluble Co-phthalocyanine with cationic groups that showed minimal aggregation and yielded high turnover frequencies.[68] Controlled potential electrolysis (CPE) experiments were only performed for 20 minutes, making it difficult to comment on any long term stability. To maximize the number of active species at the electrode interface CoPCs were immobilized on carbon-based scaffolds[22] and gas-diffusion electrodes (GDEs).[23] Interestingly, immobilization of amine-substituted CoPC on carbon nanotubes (CNTs) enables formation of methanol as the product.[69] Immobilization of CoPC on GDEs results in high current densities for the reduction of CO_2 to CO, (FE_{CO} = 95%) with a catalytic current that is stable for at least 12 h, indicating improved catalytic stability of the immobilized Co-phthalocyanine compared to homogeneous Co-phthalocyanine.

Co-phthalocyanine was immobilized in the Zr-based NU1000 MOF by attaching the catalyst to the MOF nodes by solvent-assisted ligand incorporation to form **NU1000|CoPC** (Figure **1.4**).[24] In order to investigate to which extend electron transfer between the CoPC catalyst and the NU1000 linker is of influence for catalytic performance, a Co-porphyrin was also incorporated into NU1000 to form **NU1000|Co(TPP)** via the same procedure. The observed superior activity of **NU1000|CoPC** compared to **NU1000|Co(TPP)** was attributed to a better alignment of the reduction potentials of CoPC and NU1000 than of Co(TPP) and NU1000. Reduced NU1000 can efficiently reduce cobalt in CoPC to generate the key Co^0 species, whereas a larger overpotential is necessary to reduce Co(TPP) to the same oxidation state.

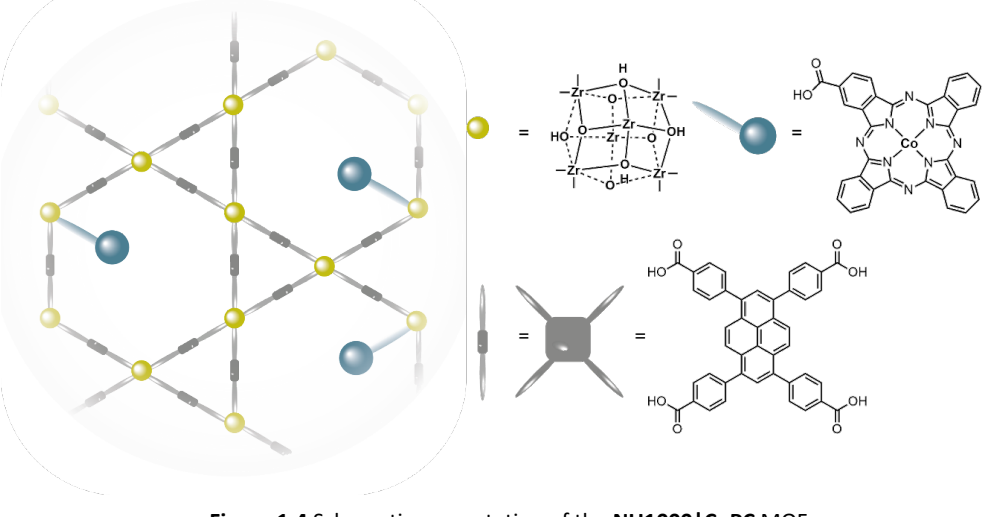

Figure 1.4 Schematic presentation of the **NU1000|CoPC** MOF.

NU1000|CoPC formed CO with faradaic efficiencies ranging from 40 to 70% for applied potentials between −0.55 V and −0.85 V vs. RHE (Table **1.*2***). In case of **NU1000|CoPC** substantially more dihydrogen was produced compared to CoPC immobilized on a GDE, which showed FE_{CO} = 95%. We anticipate this difference in faradaic efficiency for CO to be caused by slow mass transport of CO_2 in the MOF pores relative to the homogeneous system. As mass transport of CO_2 consumed during CO_2RR in MOF pores is significantly more difficult than on a GDE, where a constant flow is maintained, the lower FE_{CO} for the MOF-immobilized CoPC could be explained by a less rapid flow of CO_2 to the catalytic sites. On the other hand, it is important to note that reduced mass transport can also result in higher local pH, as protons are consumed during the CO_2RR, which would then result in a higher FE_{CO}. Not only selectivity for CO, but also catalytic currents decreased over time when using **NU1000|CoPC**. Chronoamperometry at −0.65 V vs. RHE resulted in a current of −1.75 $mAcm^{-2}$ that decreased by approximately 30% over 4 hours. In agreement with this the current densities decreased over consecutive CV scans. These observations indicate catalyst instability. As immobilization of the phthalocyanine in the MOF pore prevents aggregation, degradation of the CoPC active sites must proceed via a different mechanism than was described for homogeneous phthalocyanines. A MOF system with a Co-phthalocyanine equipped with four carboxylic acid groups as the linker and Fe-based nodes (**MOF-1992**) showed a good faradaic efficiency (FE_{CO} = 80%) and a stable catalytic current for at least two hours.[70] Both **MOF-1992** and **NU1000|CoPC** showed lower FE for CO as the product compared to homogeneous Co-phthalocyanine. Additionally, local increase of pH in the MOF pores might cause hydrolysis of the bond between the Zr-node and the CoPC, resulting in loss of the CoPC species from the MOF.

Table 1.2 Farradaic efficiency for CO for phthalocyanine-based systems.

Species	**E (V vs. RHE)**	**pH**	**FE_{CO} (%)**
CoPC on GDE[a]	−0.72	7.3	96[23]
NU1000|CoPC[b]	−0.85	8.5	44[24]
NU1000|CoPC[b]	−0.75	8.5	56[24]
NU1000|CoPC[b]	−0.65	8.5	75[24]
NU1000|CoPC[b]	−0.55	8.5	55[24]
MOF-1992[c]	−0.63	6.8	80[70]

[a] $NaHCO_3$, WE = glassy carbon, [b] $KHCO_3$, WE = graphite sheet, [c] $KHCO_3$, WE = glassy carbon.

1.4.2 $Re(bpy)(CO)_3$

$[Re(bpy)(CO)_3]$ (bpy = bipyridine) was first reported in 1984 by Lehn and coworkers and has been investigated as catalyst for the CO_2 reduction reaction ever since.[71,72] High catalytic rates and selectivity to form CO have been reported, but instability of the catalyst, caused by dimerization, is a recurring problem.[73] With this in mind, immobilization of the catalyst in a manner that prevents dimerization reactions may result in higher catalyst stability. Various ways have been explored of immobilizing this catalyst, including immobilization in liposomes, on mesoporous organosilica and on carbon electrodes as polymer thin film.[74–76]

$[Re(bpy\text{-}2,2\text{-}dicarboxylic\ acid)(CO)_3]$ catalysts were incorporated as linkers into the Zn-based MOF **Re-SURMOF** (Figure 1.5), which was grown as thin film onto an FTO substrate by lipid phase epitaxy.[77] **Re-SURMOF** was found to reduce CO_2 to CO with a high faradaic efficiency of 93% during chronoamperometry at −1.6 V vs. NHE in ethanol. The MOF film was compared to both $[Re(bpy\text{-}dicarboxylic\ acid)(CO)_3]$ in homogeneous solution as well as its drop casted form on an FTO electrode, for which lower faradaic efficiencies to CO were found of 65% for the homogeneous compound and 61% for the drop casted form (

Table 1.*3*). **Re-SURFMOF** showed higher catalytic current densities as well, which the authors attribute to the highly oriented structure of the MOF film at the electrode surface. This allows for efficient charge transport along the [001] direction of the framework, which ensures activation of catalytic sites further from the electrode surface. In contrast to the MOF system, in homogeneous solution only a limited number of catalysts are close enough to the electrode surface to be activated, and a drop cast of catalysts may be too amorphous to ensure sufficient contact with electrode and electrolyte. However, the MOF thin film showed to be instable when CA experiments were continued for more than 30 minutes, and all catalytic activity was lost within 2 hours of electrolysis. As dimerization reactions seem unlikely within the MOF, catalyst degradation reactions must proceed via a different mechanism than in homogeneous solution. XRD of the electrode after electrolysis confirmed that delamination of the MOF thin film had taken place. Possibly, the bonds between the carboxylic acid moieties of the catalyst and the Zn nodes or FTO are not stable and hydrolyze, resulting in dissolution of the entire film.[78]

Table 1.3 Faradaic efficiency for CO for Re(bpy)$(CO)_3$-based systems.

Species	E (V vs. NHE)	FE_{CO} (%)
Re-SURMOF	−1.6	93[77]
Re(bpy)$(CO)_3$ homogeneous	−1.6	65[77]
Re(bpy)$(CO)_3$ dropcasted	−1.6	61[77]

TBAH + 5% trifluoroethanol in acetonitrile, WE = FTO

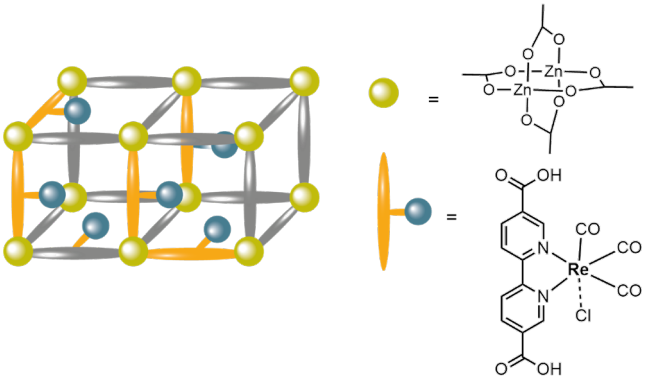

Figure 1.5 Schematic presentation of the structure of **Re-SURMOF**.

1.5 O_2 reduction catalysts in MOFs

1.5.1 Co-porphyrin

Various Co-porphyrins that can catalyze the oxygen reduction reaction (ORR) at a relatively low overpotential have been designed to direct the selectivity of ORR towards either water or hydrogen peroxide, by adding bulky groups as well as inducing electronic effects on the porphyrin ring.[78–82] Aromatic macrocycles such as porphyrins are often best described as heterogeneous catalysts as they tend to aggregate in aqueous solution, which makes them stick to the hydrophobic surface of electrode materials such as glassy carbon.[47,61] Therefore, for this type of catalysts it is especially important to determine the nature of the catalytically active species.[66,78]

Co-porphyrin was applied as the linker in the MOF **PCN-224(Co)** (Figure **1.*6***) to catalyze the ORR towards hydrogen peroxide.[48] **PCN-224(Co)** was compared to the Co-porphyrin containing linker drop casted onto an electrode and showed improved FE for hydrogen peroxide of 80%, compared to 30% for the free linker, albeit with a somewhat decreased current density. Dimers of Co-porphyrin are reported to favor H_2O as the main product, while monomeric catalytic sites often favor formation of H_2O_2. Therefore, the improved FE

was ascribed to immobilization of the catalyst in the ordered framework of the MOF, preventing dimerization of the catalytic species. Fully in line with this hypothesis is the observation that aggregation of Co-macrocycle catalysts in solution was found to decrease the selectivity and result in production of only small amounts of H_2O_2.[66]

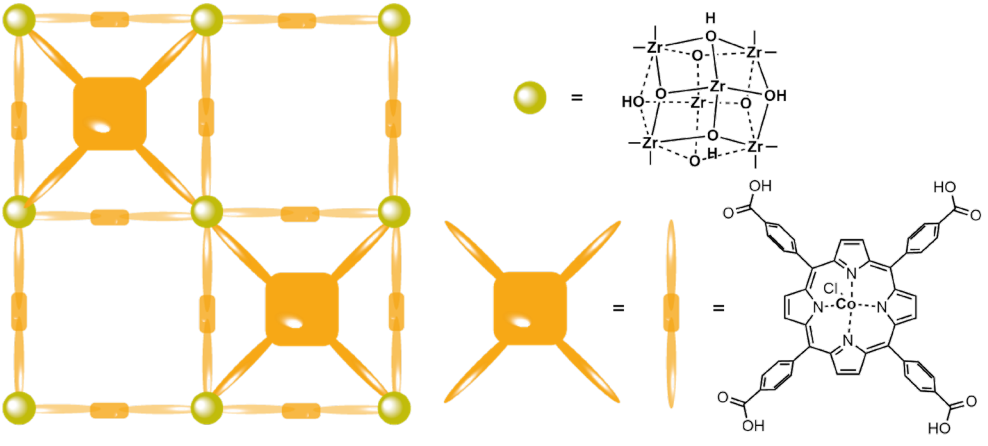

Figure 1.6 Schematic presentation of the structure of **PCN-224(Co)**.

1.6 Water oxidation catalysts in MOFs

1.6.1 [Ru(tpy)(dcbpy)(OH_2)]

The redox properties of $[Ru(tpy)(bpy)(OH_2)]^{2+}$ (tpy = terpyridine) were reported by Meyer and coworkers as early as 1983;[83] later they also started investigating the complex as a catalyst for the water-oxidation reaction.[84,85] Formation of the O-O bond at Ru-based water oxidation catalysts (WOCs) is typically the rate determining step,[86] and can proceed via an interaction between two M-O species (I2M) mechanism resulting in direct formation of O_2, or via a water nucleophilic attack (WNA) mechanism.[87] In the WNA mechanism, the O-O bond is formed by nucleophilic attack of water on a high-oxidation state M=O species. In most cases, proton transfer plays a role in the WNA mechanism. Therefore, high solvent kinetic isotope effects and buffer concentration dependent catalytic performance are good diagnostic tools for the WNA mechanism.[88] $[Ru(tpy)(bpy)(OH_2)]^{2+}$ catalysts perform water oxidation via the WNA mechanism.[85]

The first MOF-WOC was obtained by incorporation of $[Ru(tpy)(dcbpy)OH_2]^{3+}$ (dcbpy = 2,2'-bipyridine-5,5'-dicarboxylic acid) water oxidation catalysts by post synthetic ligand exchange into an UiO-67 thin film grown onto FTO, to form **UiO|[RuOH$_2$]|FTO** (Figure

1.7).[89] The MOF film exhibited water oxidation activity with a faradaic efficiency of 82% for O_2. The onset potential for water oxidation is 1.4 V vs. Ag/AgCl at pH 6 and 1.1 V vs. Ag/AgCl at pH 8. Such a pH-dependent onset potential is expected for the WNA mechanism as deprotonation of water occurs simultaneously with nucleophilic attack on the M=O species. Approximately 6% of the UiO-67 linkers were displaced by a ruthenium-functionalized linker, resulting in a number of catalytic sites immobilized on the electrode that is two orders of magnitude higher than the theoretical maximum number of catalysts that would be present in a monolayer. The reversible redox couples ascribed to the molecular ruthenium complex were observed both before and after catalysis, indicating that the catalyst is stable during these experiments. However, relatively low catalytic current densities were obtained, which was ascribed to the non-conductive nature of UiO-67 and poor charge transport that is fully dependent on electron hopping between the disperse Ru centers present on 6% of the MOF linkers. The combination of the low activity of the catalytic systems and the equivalent homogeneous systems being particularly studied in presence of sacrificial oxidants makes it difficult to estimate to which extend embedding of the ruthenium sites within the UiO-67 MOF leads to a more active catalytic species.[84,90]

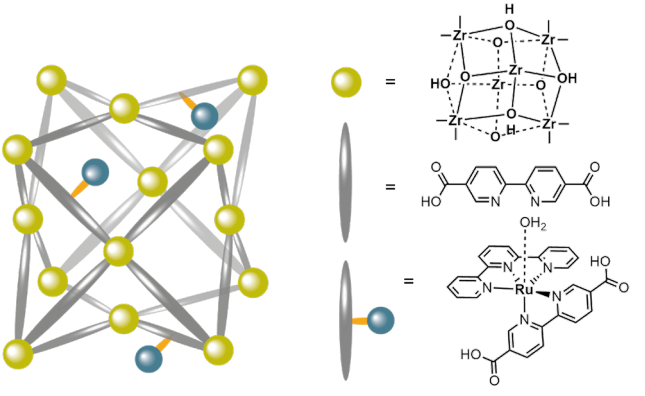

Figure 1.7 Schematic presentation of the **UiO|[RuOH$_2$]|FTO** MOF.

1.6.2 [Ru(II)(tda)(py(PhCOOH)$_2$)$_2$]

A ruthenium catalyst with a bda (H_2bda = 2,2'-bipyridine-6,6'-dicarboxylic acid) ligand was reported by the group of Sun to perform catalytic water oxidation with a very high activity.[90] The catalyst forms dimers of two Ru^{IV}-O species to form the O-O bond via the I2M mechanism. Three years later, Llobet and coworkers reported [Ru(II)(tda)(py)$_2$], (H_2tda = 2,2':6',2''-terpyridine-6,6'-dicarboxylic acid) with an even higher activity, with a TOF of 50 000 s^{-1} at pH 10 and 7700 s^{-1} at pH 7.[91] Interestingly, this catalyst forms the O-O bond through the WNA mechanism. Anchoring the catalyst to multiwalled carbon nanotubes

(MWCNTs) by functionalizing the pyridine ligand with a pyrene moiety that binds to the MWCNTs by π-π interactions, resulted in a highly stable catalyst with a TON larger than 10^7.[92]

A NU1000-type mixed linker MOF, with [Ru(II)(tda)(py(PhCOOH)$_2$)$_2$] replacing some of the TBAPy linkers (Figure **1.*8***) was developed.[50] The **NU1000|[Ru(tda)(py(PhCOOH)$_2$)$_2$]** MOF was synthesized by solvothermal synthesis with up to 30% of ruthenium linker, resulting in a maximum incorporation of almost 0.34 Ru-containing linkers per node. The [Ru(tda)(py(PhCOOH)$_2$)$_2$] catalyst can be activated by CPE at 1.4 V vs. NHE for 40 minutes, after which it oxidizes water at a potential of 1.3 V vs. NHE at neutral pH. As the 1,3,6,8-tetrakis(p-benzoic acid)pyrene (TBAPy) linkers are also oxidized at 1.3 V vs. NHE, electrons are transported from the Ru-catalyst, via the TBAPy linker to the electrode when this potential is applied. Thus, in contrast to **UiO-[RuOH$_2$]|FTO** based on the inert UiO-67 framework, the TBAPy linkers in **NU1000|[Ru(tda)(py(PhCOOH)$_2$)$_2$]** are involved in charge transfer from catalyst to electrode. **NU1000|[Ru(tda)(py(PhCOOH)$_2$)$_2$]** suspended on MWCNTs shows water oxidation activity with a faradaic efficiency for O_2 of 37%. The FE is relatively low due to oxidation of the TABPy linkers. The authors argue that better matching of the redox potentials of the TABPy linker and the ruthenium catalyst would result in a larger proportion of catalytic sites engaging in catalysis. Since oxidation of TBAPy occurs first, an initial period of CPE to oxidize all linkers followed by measuring oxygen content may lead to a possible underestimation of the FE. The catalytic activity of **NU1000|[Ru(tda)(py(PhCOOH)$_2$)$_2$]** could not be directly compared to the catalyst in solution due to solubility issues. As an alternative, [Ru(II)(tda)(py(PhCOOH)$_2$)$_2$] suspended on MWCNTs was drop casted on a glassy carbon electrode for direct comparison to the **NU1000|[Ru(tda)(py(PhCOOH)$_2$)$_2$]** MOF suspended on MWCNTs. Both the MOF and the catalyst suspended on MWCNTs showed the $Ru^{III/II}$ and $Ru^{IV/III}$ redox couples at similar potentials after activation by CPE at 1.2 V vs. NHE. The drop casted MWCNTs|[Ru(II)(tda)(py(PhCOOH)$_2$)$_2$] show a catalytic peak in CV starting at 1.4 V vs. NHE.[92] **NU1000|[Ru(tda)(py(PhCOOH)$_2$)$_2$]** on MWCTNs does not show a similar wave in CV, but measurements with a Clark electrode during CPE at 1.3 V vs. NHE showed a stable increase of formed dioxygen for 80 minutes.

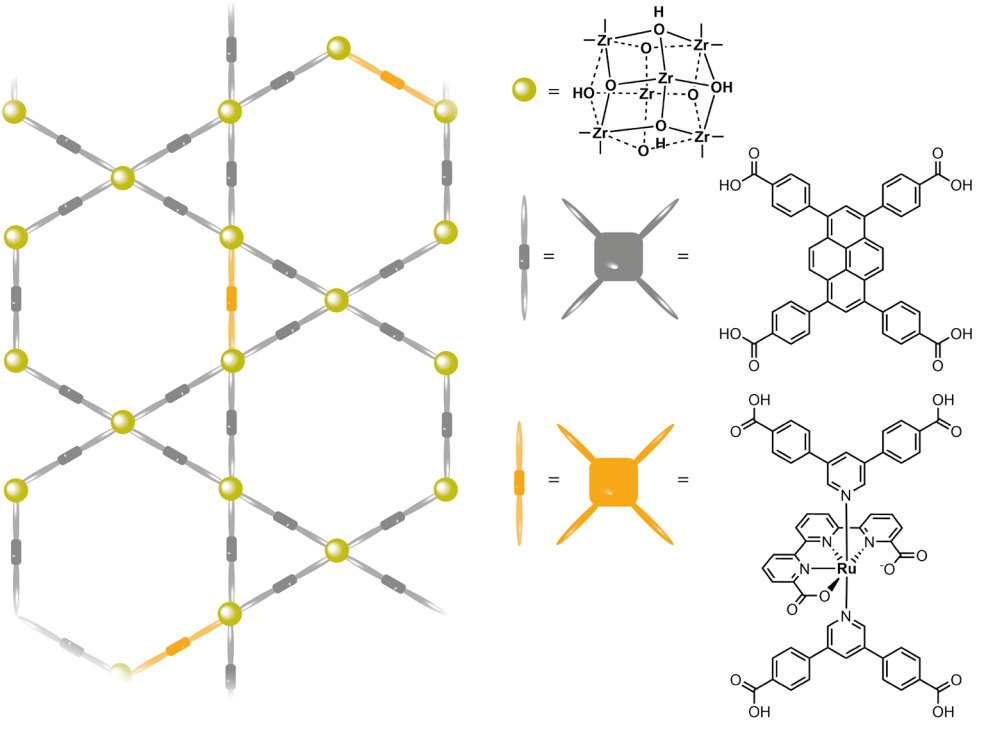

Figure 1.8 Schematic presentation of the mixed linker **NU1000|[Ru(tda)(py(PhCOOH)$_2$)$_2$]** MOF. TBAPy linkers are displayed in grey and [Ru(tda)(py(PhCOOH)$_2$)$_2$] linkers in yellow.

1.6.3 [Fe(salen)]

The Schiff base complex [Fe(salen)] has been reported as a catalyst for various reactions in organic solvents, such as oxidation of sulfides, polymerization of ethene and propene and oxidation of hydrocarbons in the presence of hypochlorite.[93–95] No [Fe(salen)] catalysts have been reported where the molecular complex is the true catalyst for the oxygen evolution reaction, but it has been reported as a precursor for CoFe-hydroxide hybrid material with water-oxidation activity.[96] In order to stabilize the [Fe(salen)] catalyst and prevent formation of metal oxides, [Fe(salen)] has been incorporated into mesoporous silica.[97] Two different [Fe(salen)] based MOFs were employed for the oxidation of sulfides.[98,99]

[Fe^{III}(salen)(H$_2$O)]$^+$ and SiW$_{12}$O$_{40}$ clusters were incorporated into the Zn^{2+}-based MOF ZIF-8 (Figure **1.*9***) to form the highly stable **FSWZ-8** composite that is active as a catalyst for the oxygen evolution reaction.[49] SiW$_{12}$O$_{40}$ is a polyoxometalate (POM) which is a well-known

electron shuttle (E^0 (POM/POM$^-$) = 0.054 V vs. NHE).[100] The composite shows high activity, with FE of 95% and an onset potential of 1.1 V vs. NHE at neutral pH. A large catalytic current was observed with a peak current density of 4 mAcm^{-2}, compared to ZIF-8 (no catalytic current) and ZIF-8 containing only [Fe^{III}-(salen)(H_2O)]$^+$ (**FSZ-8,** 2.0 mAcm^{-2}). Homogeneous [Fe^{III}(salen)(H_2O)]$^+$ showed a peak catalytic current density of 4 mAcm^{-2} that quickly decayed over consecutive scans. A high stability of the **FSWZ-8** composite was demonstrated by 500 CV cycles and CPE at 1.2 V vs. NHE for 6 hours, during which the observed current did not change over time.

Differences in UV-vis, FTIR and Raman spectra of the **FSWZ-8** material compared to those of [Fe^{III}-(salen)(H_2O)]$^+$ indicated the presence of a different species in the MOF. A CV of [Fe^{III}-(salen)(H_2O)]$^+$ in homogeneous solution shows complete disappearance of all catalytic activity over 10 cycles. Since metal oxides can easily be formed under oxidative conditions, the instability observed in CV of [Fe^{III}(salen)(H_2O)]$^+$ was explained by formation of FeO_x during catalysis.[101] Fe^{IV}=O is the active intermediate in Fe-salen catalysts and application of high potentials ensures this high oxidation state species to be constantly present in high concentrations, which may lead to degradation and formation of iron oxides.[93] In order to evaluate if FeOx species are formed in situ during OER activity of **FSWZ-8**, control experiments were undertaken with different three species of FeOx, which were investigated with CV and Tafel analysis under the same conditions. In the first control, iron nanoparticles were deposited in ZIF-8 by annealing the **FSWZ-8** at 400 °C in presence of air to form **FeOx$_{400}$Z-8**. In the second sample FeOx was deposited on a carbon-cloth (CC) electrode to form **FeO$_x$-CC,** and in the third sample iron oxide nanoparticles on ZIF-8 coated carbon-cloth electrode (labeled as **FeO$_x$-Z8**) was prepared through electrodeposition by applying high anodic potential in an aqueous solution of $FeCl_3$ (1 mM). CV experiments of these controls showed that these FeOx species had no OER activity at the potential at which **FSWZ-8** operates under the applied reaction conditions. It was therefore concluded that the OER mediated by **FSWZ-8** does not involve FeOx species. The authors attribute the stabilization of Fe-salen in the MOF to its confinement within the MOF, and the increased activity to effective charge transport involving the POM. Incorporation of the redox-active POM, with an oxidation potential at which the iron sites are oxidized, lowers the overall Ohmic resistance via a similar effect as has been described for **NU1000|CoPC** in CO_2RR.

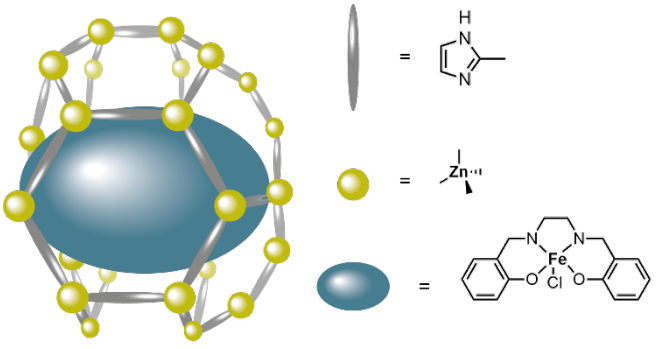

Figure 1.9 Schematic presentation of incorporation of Fe-salen into the zeolitic framework ZIF-8.

1.7 Challenges

A handful of reports have shown interesting results when a molecular electrocatalyst is incorporated into a MOF, however, the field is still quite new and several major challenges remain. The limiting factor for catalytic reactions can be found in 1) slow electron transport, 2) slow mass transport of reactants and products, or 3) low activity of the catalytic site itself, either caused by the confinement effects, or an unfavorable electronic structure when integrated within the MOF. Some of these limitations are issues that are encountered by many scientists working on metal-organic frameworks, while others are not frequently discussed in the field but should be considered.

Issues relating to electron transfer in MOFs belong to the first category. Electron transfer in MOFs can proceed via diffusional charge transfer through π-π stacking of aromatic moieties,[102,103] electron transfer through bonds,[104,105] or cation-coupled electron hopping between redox-active guests or linkers.[106–108] When electrons are transferred by π-π stacking of aromatic moieties, delocalized electrons are shared between the stacked aromatic rings. This form of charge transport requires close proximity of linkers in parallel planes and has a conductivity of typically 10^{-4} S cm^{-1}. Dinca and coworkers showed Ga, Ni and Co MOFs with the linker 2,3,6,7,10,11-hexahydroxytriphenylene (H_6HOTP) to exhibit similar conductivities of around 3×10^{-3} S cm^{-1}.[102] Electron transfer through bonds is a form of intervalence charge transport and depends on orbital overlap. It is the fastest form of charge transport in MOFs with a conductivity of typically 1 S cm^{-1}. In the MOF $Fe(tri)_2(BF_4)_x$ (tri^- = 1,2,3-triazolate; x = 0.09, 0.22, and 0.33), electrons are transported by conjugation of the triazolate linker π-orbitals and the 3d orbitals of the iron centers.[105]

Cation-coupled electron hopping depends on the distance between two electro-active moieties as well as the diffusion of cations. Cation-coupled electron hopping rates can be determined by Cottrell analysis of CPE measurements and typically reaches conductivities of 10^{-10}-10^{-12} S cm^{-1}. The difference in electronic conductivity caused by the through-bond, π-π stacking and electron hopping mechanisms is notable, and improving electron-hopping rates is a major topic of investigation.[106] Even though redox-active MOFs can be used to enhance charge propagation, matching the potentials of redox-active sites and catalysts within the MOF is crucial as discrepancies in redox potentials will lead to slow electron-transfer processes. When the redox potential of the linker is more negative than the redox potential of the catalyst, either the linkers are not reduced and form a redox-innocent framework, or the catalytic reaction can only be performed at a high overpotential, where also the linker is reduced. On the other hand, if the redox potential of the catalyst is much more negative than the redox potential of the linker, the linker will not be able to reduce the catalyst and will likely accumulate electrons without passing them on to the catalyst. It is also important to note that charge propagation studies are often performed in DMF or other organic solvents, while for catalytic purposes for a green energy economy water is usually the preferred solvent and charge propagation rates and mechanisms may vary with solvent polarity.[106,109,110] Additionally, when charge transport in MOFs is coupled to ion migration in aqueous electrolyte, it is not far-fetched to assume that proton-coupled electron transfer is involved. In this case, electron transfer rates may be directly dependent on the electrolyte pH and the pKa values of nodes and linkers. Furthermore, an appropriate electronic connection between the support and the MOF is expected to be essential for good electron transport as well. The method in which the MOF is immobilized (e.g. as a carbon black–Nafion ink or directly grown on FTO) as well as potential defects that accompany anchoring of the MOFs are likely important factors to consider when studying electron transfer in MOFs.

Apart from charge transport issues, the stability of MOFs is a topic of concern. Often, changes in morphology of MOFs or complete delamination of MOF thin films are observed during catalysis.[77,89,111] For example, the **Re-SURMOF** thin film grown on FTO for CO_2 reduction completely delaminated,[77] and in the case of Cu-adeninato MOF (Cu-ade-MOF) SEM images before and after electrolysis showed morphology changed completely after CO_2 reduction electrolysis.[111] A strategy for improving stability of MOFs grown directly onto FTO substrates would be to create a monolayer of the node material, such as ZnO, by atomic-layer deposition (ALD) onto the FTO substrate, which then can be used as a platform

to grow more stable FTO|MOF structures.[112,113] This strategy may avoid unstable bonds between linkers and FTO, resulting in MOF delamination. Mechanisms of catalyst degradation are rarely investigated, making it difficult to know whether degradation is triggered by redox reactions occurring at high potentials, or by chemical reactions involving solvents or products formed. Good stability in a wide pH range is essential for MOFs used in reactions such as water oxidation, dihydrogen evolution and CO_2 reduction. These reactions may result in significant pH gradients in the MOF pores, particularly if proton transport is slow. As improving the stability of homogeneous catalysts is one of the main motivations for their incorporation into a MOF, it is imperative to investigate the mechanisms of MOF degradation. Given that a local pH variation to alkaline and acidic conditions is expected for reduction and oxidation reactions, respectively, we recommend taking into account such pH variations when selecting a suitable MOF to accommodate an electrocatalyst. Additionally, whether the homogeneity of the molecular electrocatalyst is retained when embedded in a MOF, is widely overlooked.

At present mass transport in MOFs is still poorly understood. For example, the effect of rotating an electrode on mass transport inside the framework has not been reported. Mass transport to the electrode surface is increased in electrochemical setups with rotating electrodes, as well as in setups with gas diffusion electrodes and in flow cells. Thus, when using rotating electrodes mass transport to the MOF-electrolyte interface is also increased. However, whether and to what extent this affects mass transport within pores remains unclear to this date. Additionally, it has not yet been investigated what the effects are of partially blocked pores due to incorporated catalysts, interpenetrated MOF structures,[114] or MOF defects on the MOF porosity and mass transport within the MOF. Morris and coworkers have shown that ion diffusion is rate limiting in charge transport rather than electron hopping rates in organic solvent, and that charge transfer rate through MOFs increases with increasing pore sizes.[115] Related to this, the exact location where catalysis occurs is often not clear, particularly when only a small fraction of sites is catalytically active. Using mathematical reaction-diffusion models, Ott and coworkers described how a catalytic current can be limited by mass transport or charge transport.[116] They showed that when mass transport is limiting, the reactants will be consumed by catalysts at the MOF-electrolyte interface and catalysts deeper into the framework are not catalytically active. When electron transport is limiting, catalysts located far from the electrode surface will not be activated and catalysis will take place close to the electrode-MOF interface. They also showed that the optimal thickness of the catalytic MOF depends on the intrinsic activity of

the catalyst: when a relatively slow catalyst is used, a thicker MOF film, containing more catalytic sites, can be used as there is enough time for the substrate to diffuse through the pores to catalysts deeper in the framework. When a catalyst is very active, the optimal MOF film thickness is smaller as diffusion will be slower than the reaction. These models can be used to design MOFs with optimized pore structure and film thickness for substrate and charge diffusion.

A challenge that is usually overlooked but that we consider highly important to discuss is the fact that still very little is known about the effect that confinement within a MOF has on a molecular catalyst. The catalytic mechanisms of homogeneous catalysts are often only studied in homogeneous solutions, and not in the MOF. It is assumed that the mechanism by which the catalyst operates, and the catalytic species present, do not change when a catalyst is confined in a framework. This is not necessarily correct. Which reaction pathway is dominant often is very much dependent on the concentration of reactants, and thus on mass transport through the MOF. And as illustrated above, particularly local pH swings are expected to play a significant role in MOF electrochemistry. These local pH effects can in turn have many effects on catalytic mechanisms and decomposition pathways. Rarely the catalytic results of MOF-embedded catalysts are directly compared to those obtained for the homogeneous catalyst under identical conditions. This makes it difficult to judge the effectiveness of confinement of the catalyst, and to truly identify the potential of the field of electrocatalysis employing MOFs. We therefore emphasize that detailed mechanistic studies carried out for catalysts within the confinement of MOFs are indispensable to bring the field of MOF electrocatalysis to a more developed stage.

1.8 Aim and outline of this thesis

The confinement of molecular catalysts in metal-organic frameworks has the potential to lead to significant improvements in selectivity, long term activity and catalyst stability. The efficiency of electrocatalysis in MOFs is expected to be limited by either the activity of the catalyst, mass transport through the framework or electron transfer. Although initial strategies to improve electron transfer throughout MOFs have been described, major knowledge gaps still exist. For example, it remains unclear how electron transport in MOFs affects electrocatalysis and how mass transport of reactants limits electrocatalysis, and what the effects are of confinement in a MOF on the catalyst structure. It is expected that these research questions remain an important area of research in the future. The research

described in this thesis concerns the oxygen-reduction catalyst Cu-tmpaCOOH confined in MOFs. The Cu-tmpa catalyst and its catalytic performance are well characterized.[117–119] The main challenge regarding this catalyst concerns its long-term stability, which may be improved through immobilization in MOFs. The research described in this thesis addresses a number of the challenges mentioned in Section 1.7. In Chapter 2 the effect is discussed of incorporation of the Cu-tmpaCOOH catalyst in a MOF on its catalytic activity and selectivity. In Chapter 3 the effect of confinement on the catalyst itself is described. The homogeneity of the catalyst and the identity of the true active species are discussed. Chapter 4 discusses the effect of electron transport through the MOF on the catalyst and its catalytic performance. This chapter provides a comparison between a redox inert MOF and a MOF containing redox-active linkers. The efficiency of electron transfer to the catalyst, the homogeneity of the catalyst and catalytic activity and selectivity have been investigated. Chapter 5 contains a detailed discussion of the effect of pH on charge transport in redox active MOFs. Chapter 6 provides a summary of the results in this thesis as well as a conclusion and outlook.

1.9 References

[1] P. B. Duffy, C. B. Field, N. S. Diffenbaugh, S. C. Doney, Z. Dutton, S. Goodman, L. Heinzerling, S. Hsiang, D. B. Lobell, L. J. Mickley, S. Myers, S. M. Natali, C. Parmesan, S. Tierney, A. P. Williams, *Science (1979)* **2019**, *363*.

[2] M. T. Richardson, *Geophys Res Lett* **2022**, *49*, e2021GL095782.

[3] International Energy Agency, "Global energy demand rose by 2.3% in 2018, its fastest pace in the last decade - News - IEA," can be found under https://www.iea.org/news/global-energy-demand-rose-by-23-in-2018-its-fastest-pace-in-the-last-decade, **n.d.**

[4] D. S. Ginley, D. Cohen, *Fundamentals of Materials for Energy and Environmental Sustainability*, Cambridge University Press, **2011**.

[5] K. E. Dalle, J. Warnan, J. J. Leung, B. Reuillard, I. S. Karmel, E. Reisner, *Chem Rev* **2019**, *119*, 2752–2875.

[6] "What are eFuels? - eFuel Alliance," can be found under https://www.efuel-alliance.eu/efuels/what-are-efuels, **n.d.**

[7] G. Centi, S. Perathoner, *Catal Today* **2022**, *387*, 216–223.

[8] S. Perathoner, G. Centi, *Catal Today* **2019**, *330*, 157–170.

[9] Z. Cui, W. Jiao, Z. Y. Huang, G. Chen, B. Zhang, Y. Han, W. Huang, *Small* **2023**, *19*, 2301465.

[10] G. Gao, G. Zhu, X. Chen, Z. Sun, A. Cabot, *ACS Nano* **2023**, *17*, 20804–20824.

[11] W. Ma, X. Zhang, W. Li, M. Jiao, L. Zhang, R. Ma, Z. Zhou, *Nanoscale* **2023**, *15*, 11759–11776.

[12] L. Du, L. Xing, G. Zhang, M. Dubois, S. Sun, L. Du, G. Zhang, S. Sun, L. Xing, M. Dubois, *Small Methods* **2020**, *4*, 2000016.

[13] H. Wu, C. Feng, L. Zhang, J. Zhang, D. P. Wilkinson, *Electrochemical Energy Reviews 2021 4:3* **2021**, *4*, 473–507.

[14] M. Kondo, H. Tatewaki, S. Masaoka, *Chem Soc Rev* **2021**, *50*, 6790–6831.

[15] J. Li, C. A. Triana, W. Wan, D. P. Adiyeri Saseendran, Y. Zhao, S. E. Balaghi, S. Heidari, G. R. Patzke, *Chem Soc Rev* **2021**, *50*, 2444–2485.

[16] J. D. Blakemore, R. H. Crabtree, G. W. Brudvig, *Chem Rev* **2015**, *115*, 12974–13005.

[17] Y. Y. Birdja, E. Pérez-Gallent, M. C. Figueiredo, A. J. Göttle, F. Calle-Vallejo, M. T. M. Koper, *Nat Energy* **2019**, *4*, 732–745.

[18] S. Nitopi, E. Bertheussen, S. B. Scott, X. Liu, A. K. Engstfeld, S. Horch, B. Seger, I. E. L. Stephens, K. Chan, C. Hahn, J. K. Nørskov, T. F. Jaramillo, I. Chorkendorff, *Chem Rev* **2019**, *119*, 7610–7672.

[19] D. Sun, X. Xu, Y. Qin, S. P. Jiang, Z. Shao, *ChemSusChem* **2020**, *13*, 39–58.

[20] J. T. Feaster, C. Shi, E. R. Cave, T. Hatsukade, D. N. Abram, K. P. Kuhl, C. Hahn, J. K. Nørskov, T. F. Jaramillo, *ACS Catal* **2017**, *7*, 4822–4827.

[21] Q. Feng, Y. Sun, X. Gu, Z. Dong, *Electrocatalysis* **2022**, *13*, 675–690.

[22] C. L. Rooney, M. Lyons, Y. Wu, G. Hu, M. Wang, C. Choi, Y. Gao, C. W. Chang, G. W. Brudvig, Z. Feng, H. Wang, *Angewandte Chemie International Edition* **2024**, *63*, e202310623.

[23] M. Wang, K. Torbensen, D. Salvatore, S. Ren, D. Joulié, F. Dumoulin, D. Mendoza, B. Lassalle-Kaiser, U. Işci, C. P. Berlinguette, M. Robert, *Nature Communications* **2019**, *10*, 1–8.

[24] X. Li, S. Rajasree, V. Gude, Sreehari, K. Maindan, P. Deria, *Angewandte Chemie International Edition* **2023**, e202219046.

[25] J. Shen, R. Kortlever, R. Kas, Y. Y. Birdja, O. Diaz-Morales, Y. Kwon, I. Ledezma-Yanez, K. J. P. Schouten, G. Mul, M. T. M. Koper, *Nat Commun* **2015**, *6*, 1–8.

[26] M. Usman, M. Humayun, M. D. Garba, L. Ullah, Z. Zeb, A. Helal, M. H. Suliman, B. Y. Alfaifi, N. Iqbal, M. Abdinejad, A. A. Tahir, H. Ullah, *Nanomaterials* **2021**, *11*, 2029.

[27] T. Atoguchi, A. Aramata, A. Kazusakab, M. Enyoa, *J. Chem. Soc., Chem. Commun* **1991**, 156–157.

[28] G. Ramírez, G. Ferraudi, Y. Y. Chen, E. Trollund, D. Villagra, *Inorganica Chim Acta* **2009**, *362*, 5–10.

[29] A. A. Gewirth, J. A. Varnell, A. M. Diascro, *Chem Rev* **2018**, *118*, 2313–2339.

[30] S. Zhao, Y. Yang, Z. Tang, *Angewandte Chemie International Edition* **2022**, *61*, e202110186.

[31] D. J. Cole-Hamilton, R. P. Tooze, in *Catalyst Separation, Recovery and Recycling* (Eds.: D.J. Cole-Hamilton, R.P. Tooze), Springer Netherlands, **2006**, pp. 1–8.

[32] J. Wang, S. Dou, X. Wang, *Sci Adv* **2021**, *7*, 3989–4015.

[33] S. Iniyan, J. Ren, S. Deshmukh, K. Rajeswaran, G. Jegan, H. Hou, V. Suryanarayanan, V. Murugadoss, M. Kathiresan, Ben, B. Xu, Z. Guo, *The Chemical Record* **2023**, *23*, e202300317.

[34] N. F. Suremann, B. D. McCarthy, W. Gschwind, A. Kumar, B. A. Johnson, L. Hammarström, S. Ott, *Chem Rev* **2023**, *123*, 6545–6611.

[35] Y. Peng, S. Sanati, A. Morsali, H. García, S. Sanati, P. Hermenegildo García, P. A. Morsali, *Angewandte Chemie International Edition* **2022**, *62*, e202214707.

[36] S. Hindocha, *The Chemistry of Metal-Organic Frameworks: Synthesis, Characterization, and Applications*, **2017**.

[37] J. Linnemann, K. Kanokkanchana, K. Tschulik, *ACS Catal* **2021**, *11*, 5318–5346.

[38] K. Hemmer, M. Cokoja, R. A. Fischer, *ChemCatChem* **2021**, *13*, 1683–1691.

[39] V. Mouarrawis, R. Plessius, J. I. van der Vlugt, J. N. H. Reek, *Front Chem* **2018**, *6*, 623.

[40] Y. Wang, H. Cui, Z. W. Wei, H. P. Wang, L. Zhang, C. Y. Su, *Chem Sci* **2016**, *8*, 775–780.

[41] C. De Wu, M. Zhao, *Advanced Materials* **2017**, *29*, 1605446.

[42] L. Mitchell, P. Williamson, B. Ehrlichov, A. E. Anderson, V. R. Seymour, S. E. Ashbrook, N. Acerbi, L. M. Daniels, R. I. Walton, M. L. Clarke, P. A. Wright, *Chemistry – A European Journal* **2014**, *20*, 17185–17197.

[43] M. O. Cichocka, Z. Liang, D. Feng, S. Back, S. Siahrostami, X. Wang, L. Samperisi, Y. Sun, H. Xu, N. Hedin, H. Zheng, X. Zou, H. C. Zhou, Z. Huang, *J Am Chem Soc* **2020**, *142*, 15386–15395.

[44] T. F. Liu, D. Feng, Y. P. Chen, L. Zou, M. Bosch, S. Yuan, Z. Wei, S. Fordham, K. Wang, H. C. Zhou, *J Am Chem Soc* **2015**, *137*, 413–419.

[45] Y. Wang, L. Ling, W. Zhang, J. Guo, K. Ding, W. Duan, B. Liu, *Chemistry of Materials* **2019**, *31*, 9546–9553.

[46] S. Pullen, S. Roy, S. Ott, *Chemical Communications* **2017**, *53*, 5227–5230.

[47] M. E. Hoefnagel, D. Rademaker, D. G. H. Hetterscheid, *ChemSusChem* **2023**, *16*, e202300392.

[48] D. Rademaker, S. Tanase, H. Kang, J. Hofmann, D. Hetterscheid, *Chemistry – A European Journal* **2024**, e202401339.

[49] S. Mukhopadhyay, O. Basu, A. Kar, S. K. Das, *Inorg Chem* **2020**, *59*, 472–483.

[50] A. Howe, T. Liseev, M. Gil-Sepulcre, C. Gimbert-Suriñach, J. Benet-Buchholz, A. Llobet, S. Ott, *Mater Adv* **2022**, *3*, 4227–4234.

[51] I. Hod, W. Bury, D. M. Karlin, P. Deria, C.-W. Kung, M. J. Katz, M. So, B. Klahr, D. Jin, Y.-W. Chung, T. W. Odom, O. K. Farha, J. T. Hupp, I. Hod, W. Bury, D. M. Karlin, P. Deria, C. W. Kung, M. J. Katz, M. So, B. Klahr, T. W. Odom, O. K. Farha, J. T. Hupp, D. Jin, Y. Chung, *Advanced Materials* **2014**, *26*, 6295–6300.

[52] S. Roy, Z. Huang, A. Bhunia, A. Castner, A. K. Gupta, X. Zou, S. Ott, *J Am Chem Soc* **2019**, *141*, 15942–15950.

[53] C. Costentin, S. Drouet, M. Robert, J. M. Savéant, *J Am Chem Soc* **2012**, *134*, 11235–11242.

[54] B. D. McCarthy, A. M. Beiler, B. A. Johnson, T. Liseev, A. T. Castner, S. Ott, *Coord Chem Rev* **2020**, *406*.

[55] J. Calbo, M. J. Golomb, A. Walsh, *J Mater Chem A Mater* **2019**, *7*, 16571–16597.

[56] J. L. Dempsey, B. S. Brunschwig, J. R. Winkler, H. B. Gray, *Acc Chem Res* **2009**, *42*, 1995–2004.

[57] N. Kaeffer, M. Chavarot-Kerlidou, V. Artero, *Acc Chem Res* **2015**, *48*, 1286–1295.

[58] E. B. Hulley, P. T. Wolczanski, E. B. Lobkovsky, *J Am Chem Soc* **2011**, *133*, 18058–18061.

[59] N. M. Muresan, J. Willkomm, D. Mersch, Y. Vaynzof, E. Reisner, *Angewandte Chemie International Edition* **2012**, *51*, 12749–12753.

[60] S. Donck, J. Fize, E. Gravel, E. Doris, V. Artero, *Chemical Communications* **2016**, *52*, 11783–11786.

[61] B. Reuillard, J. Warnan, J. J. Leung, D. W. Wakerley, E. Reisner, *Angewandte Chemie International Edition* **2016**, *55*, 3952–3957.

[62] S. Troppmann, B. König, *Chemistry - A European Journal* **2014**, *20*, 14570–14574.

[63] N. Kaeffer, A. Morozan, J. Fize, E. Martinez, L. Guetaz, V. Artero, *ACS Catal* **2016**, *6*, 3727–3737.

[64] R. C. Klet, Y. Liu, T. C. Wang, J. T. Hupp, O. K. Farha, *J Mater Chem A Mater* **2016**, *4*, 1479–1485.

[65] P. J. Celis-Salazar, C. C. Epley, S. R. Ahrenholtz, W. A. Maza, P. M. Usov, A. J. Morris, *Inorg Chem* **2017**, *56*, 13741–13747.

[66] M. Zhu, R. Ye, K. Jin, N. Lazouski, K. Manthiram, *ACS Energy Lett* **2018**, *3*, 1381–1386.

[67] Y. Wu, G. Hu, C. L. Rooney, G. W. Brudvig, H. Wang, *ChemSusChem* **2020**, *13*, 6296–6299.

[68] S. E. Lawson, R. J. Roberts, D. B. Leznoff, J. J. Warren, *J Am Chem Soc* **2024**, *146*, 22306–22317.

[69] J. Li, B. Shang, Y. Gao, S. Cheon, C. L. Rooney, H. Wang, *Nature Synthesis* **2023**, *2*, 1194–1201.

[70] R. Matheu, E. Gutierrez-Puebla, M. Á. Monge, C. S. Diercks, J. Kang, M. S. Prévot, X. Pei, N. Hanikel, B. Zhang, P. Yang, O. M. Yaghi, *J Am Chem Soc* **2019**, *141*, 17081–17085.

[71] J. Hawecker, J. M. Lehn, R. Ziessel, *J Chem Soc Chem Commun* **1984**, 328–330.

[72] F. P. a Johnson, M. W. George, F. Hartl, J. J. Turner, *Organometallics* **1996**, *15*, 3374–3387.

[73] E. E. Benson, C. P. Kubiak, *Chemical Communications* **2012**, *48*, 7374–7376.

[74] D. M. Klein, S. Rodríguez-Jiménez, M. E. Hoefnagel, A. Pannwitz, A. Prabhakaran, M. A. Siegler, T. E. Keyes, E. Reisner, A. M. Brouwer, S. Bonnet, *Chemistry – A European Journal* **2021**, *27*, 17203–17212.

[75] M. Waki, K. I. Yamanaka, S. Shirai, Y. Maegawa, Y. Goto, Y. Yamada, S. Inagaki, *Chemistry – A European Journal* **2018**, *24*, 3846–3853.

[76] A. Zhanaidarova, A. L. Ostericher, C. J. Miller, S. C. Jones, C. P. Kubiak, *Organometallics* **2019**, *38*, 1204–1207.

[77] L. Ye, J. Liu, Y. Gao, C. Gong, M. Addicoat, T. Heine, C. Wöll, L. Sun, *J Mater Chem A Mater* **2016**, *4*, 15320–15326.

[78] Y. Wei, L. Zhao, Y. Liang, M. Yuan, Q. Wu, Z. Xue, X. Qiu, J. Zhang, *Chemical Engineering Journal* **2023**, *476*, 146575.

[79] R. Zhang, J. J. Warren, *J Am Chem Soc* **2020**, *142*, 13426–13434.

[80] Y. Liu, G. Zhou, Z. Zhang, H. Lei, Z. Yao, J. Li, J. Lin, R. Cao, *Chem Sci* **2019**, *11*, 87–96.

[81] A. N. Oldacre, M. R. Crawley, A. E. Friedman, T. R. Cook, *Chemistry – A European Journal* **2018**, *24*, 10984–10987.

[82] T. Kuwana, R. J. H. Chan, Y. O. Su, *Inorg Chem* **1985**, *24*, 3777–3784.

[83] K. J. Takeuchi, M. S. Thompson, D. W. Pipes, T. J. Meyer, *Inorg Chem* **1983**, *23*, 1845–1851.

[84] J. J. Concepcion, J. W. Jurss, J. L. Templeton, T. J. Meyer, *J Am Chem Soc* **2008**, *130*, 16462–16463.

[85] J. J. Concepcion, J. W. Jurss, M. K. Brennaman, P. G. Hoertz, A. O. T. Patrocinio, N. Y. Murakami Iha, J. L. Templeton, T. J. Meyer, *Acc Chem Res* **2009**, *42*, 1954–1965.

[86] A. M. Angeles-Boza, J. P. Roth, *Inorg Chem* **2012**, *51*, 4722–4729.

[87] R. Matheu, M. Z. Ertem, C. Gimbert-Suriñach, X. Sala, A. Llobet, *Chem Rev* **2019**, *119*, 3453–3471.

[88] Z. Chen, J. J. Concepcion, X. Hu, W. Yang, P. G. Hoertz, T. J. Meyer, *Proc Natl Acad Sci U S A* **2010**, *107*, 7225–7229.

[89] B. A. Johnson, A. Bhunia, S. Ott, *Dalton Transactions* **2017**, *46*, 1382–1388.

[90] L. Duan, F. Bozoglian, S. Mandal, B. Stewart, T. Privalov, A. Llobet, L. Sun, *Nature Chemistry 2012 4:5* **2012**, *4*, 418–423.

[91] R. Matheu, M. Z. Ertem, J. Benet-Buchholz, E. Coronado, V. S. Batista, X. Sala, A. Llobet, *J Am Chem Soc* **2015**, *137*, 10786–10795.

[92] J. Creus, R. Matheu, I. Peñafiel, D. Moonshiram, P. Blondeau, J. Benet-Buchholz, J. García-Antón, X. Sala, C. Godard, A. Llobet, *Angewandte Chemie International Edition* **2016**, *55*, 15382–15386.

[93] V. K. Sivasubramanian, M. Ganesan, S. Rajagopal, R. Ramaraj, *Journal of Organic Chemistry* **2002**, *67*, 1506–1514.

[94] T. Kurahashi, Y. Kobayashi, S. Nagatomo, T. Tosha, T. Kitagawa, H. Fujii, *Inorg Chem* **2005**, *44*, 8156–8166.

[95] K. C. Gupta, A. K. Sutar, *Coord Chem Rev* **2008**, *252*, 1420–1450.

[96] J. Du, G. Liu, F. Li, Y. Zhu, L. Sun, *Advanced Science* **2019**, *6*, 1900117.

[97] R. L. Oliveira, T. Nijholt, M. Shakeri, P. E. De Jongh, R. J. M. K. Gebbink, K. P. De Jong, *Catal Sci Technol* **2016**, *6*, 5124–5133.

[98] J. Li, J. Yang, Y. Y. Liu, J. F. Ma, *Chemistry – A European Journal* **2015**, *21*, 4413–4421.

[99] Z. Yang, C. Zhu, Z. Li, Y. Liu, G. Liu, Y. Cui, *Chemical Communications* **2014**, *50*, 8775–8778.

[100] J. Lee, J. Kim, W. Choi, *Environ Sci Technol* **2007**, *41*, 3335–3340.

[101] M. A. Asraf, H. A. Younus, M. Yusubov, F. Verpoort, *Catal Sci Technol* **2015**, *5*, 4901–4925.

[102] G. Skorupskii, G. Chanteux, K. N. Le, I. Stassen, C. H. Hendon, M. Dincă, *Ann N Y Acad Sci* **2022**, *1518*, 226–230.

[103] T. C. Narayan, T. Miyakai, S. Seki, M. Dincă, *J Am Chem Soc* **2012**, *134*, 12932–12935.

[104] F. Gándara, F. J. Uribe-Romo, D. K. Britt, H. Furukawa, L. Lei, R. Cheng, X. Duan, M. O'Keeffe, O. M. Yaghi, *Chemistry – A European Journal* **2012**, *18*, 10595–10601.

[105] J. G. Park, M. L. Aubrey, J. Oktawiec, K. Chakarawet, L. E. Darago, F. Grandjean, G. J. Long, J. R. Long, *J Am Chem Soc* **2018**, *140*, 8526–8534.

[106] A. T. Castner, H. Su, E. Svensson Grape, A. K. Inge, B. A. Johnson, M. S. G. Ahlquist, S. Ott, *J Am Chem Soc* **2022**, *144*, 5910–5920.

[107] Muhammad Abbas, A. M. Marti, Arslan Umer, Monu Joy, Ya-Ching Yang, Sue-Lein Wang, K. J. Balkus, *New Journal of Chemistry* **2023**, *47*, 21159–21167.

[108] P. A. Herrera-Herrera, E. Rodríguez-Sevilla, A. S. Varela, *Dalton Transactions* **2021**, *50*, 16939–16944.

[109] J. Li, A. Kumar, S. Ott, *J Am Chem Soc* **2024**, *146 (17)*, 12000–12010.

[110] J. Li, A. Kumar, B. A. Johnson, S. Ott, *Nat Commun* **2023**, *14*, 1–10.

[111] F. Yang, A. Chen, P. L. Deng, Y. Zhou, Z. Shahid, H. Liu, B. Y. Xia, *Chem Sci* **2019**, *10*, 7975–7981.

[112] S. Goswami, M. Rimoldi, R. Anderson, C. Lee, X. Li, A. Li, P. Deria, L. X. Chen, R. D. Schaller, D. A. Gómez-Gualdrón, O. K. Farha, J. T. Hupp, *Chemistry of Materials* **2022**, *34*, 9446–9454.

[113] K. B. Lausund, O. Nilsen, *Nat Commun* **2016**, *7*, 1–9.

[114] B. A. Johnson, A. Bhunia, H. Fei, S. M. Cohen, S. Ott, *J Am Chem Soc* **2018**, *140*, 2985–2994.

[115] M. Cai, Q. Loague, A. J. Morris, *Journal of Physical Chemistry Letters* **2020**, *11*, 702–709.

[116] B. A. Johnson, A. M. Beiler, B. D. McCarthy, S. Ott, *J Am Chem Soc* **2020**, *142*, 11941–11956.

[117] M. Langerman, D. G. H. Hetterscheid, *Angewandte Chemie International Edition* **2019**, *58*, 12974–12978.

[118] M. Langerman, D. G. H. Hetterscheid, *ChemElectroChem* **2021**, *8*, 2783–2791.

[119] P. H. van Langevelde, D. G. H. Hetterscheid, *Chem Catalysis* **2024**, *4*, 101069.